Thermochimica Acta, 154 (1989) 355–365
Elsevier Science Publishers B.V., Amsterdam – Printed in The Netherlands

KINETIC STUDIES OF RAPID OIL SHALE PYROLYSIS I. TEMPERATURE CHARACTERIZATION AND FLOW VISUALIZATION IN A LAMINAR FLOW ENTRAINED REACTOR

MING-SHING SHEN, LAWRENCE J. SHADLE and JOHN J. KOVACH

U.S. Department of Energy, P.O. Box 880, Morgantown, WV 26507-0880 (U.S.A.)

GUO-QING ZHANG and RICHARD A. BAJURA

Department of Mechanical and Aerospace Engineering, West Virginia University, Morgantown, WV 26506 (U.S.A.)

(Received 28 March 1989)

ABSTRACT

An entrained reactor system has been used to study the kinetics of oil shale pyrolysis. The temperature environment and the entraining gas flow are critical parameters in determining the shale particle temperature and the shale flow rate. Shale particle temperature and shale flow rate must be determined in order to measure the kinetics of oil shale pyrolysis. The temperatures of the furnace walls and the entraining gas were independently controlled to enable isothermal operation. A cluster thermocouple consisting of three thermocouples, each of a different bead size, was used to test for a possible discrepancy between radiative heat transfer from the hot walls and convective heat transfer from the hot gas. A simple mathematical model has been developed to calculate the gas and wall temperatures, based on temperature measurements of the three thermocouples. Flow visualization shows that proper inlet design and operating conditions are essential in order to prevent dispersion of shale particles and ensure uniform treatment conditions for all particles. This is particularly true for laminar flow, where particle velocity can vary with variations in the radius of the reactor tube. Turbulent, unsteady laminar and steady laminar flow regimes have been visually characterized at different flow ratios and Reynolds numbers.

INTRODUCTION

Recent interest in oil shale research has been concerned with high heating rate oil shale pyrolysis. The use of entrained flow reactors in rapid oil shale pyrolysis has been very limited [1–3]. The primary purpose of past research using high heating rate pyrolysis has been to produce higher yields of liquid and gaseous hydrocarbon products than is possible using conventional, slow heating rate pyrolysis. However, most of the kinetic rate data available in the literature were generated using slow heating rate pyrolysis. The present laminar flow entrained reactor (LFER) system was designed by carefully

0040-6031/89/$03.50 © 1989 Elsevier Science Publishers B.V.

considering typical problems encountered by past researchers who did not attempt to measure particle temperatures and velocities, and were therefore unable to generate kinetic rate data. The temperature environment and the entraining gas flow are both critical parameters in determining the shale particle temperature and the shale flow rate. Careful inlet design and appropriate operating conditions [4] are essential in order to ensure uniform treatment conditions for all particles. Flow visualization studies should be performed to characterize the degree of dispersion of shale particles in the entrained flow reactor, and to establish the regions of stable flow. To ensure isothermal operation of the system, a bundle of three thermocouples, each of a different bead size, was used to test for a possible discrepancy between radiative heat transfer from the hot walls and convective heat transfer from the hot gas. A simple mathematical model for laminar flow was developed to estimate gas and reactor wall temperatures, and to allow for their adjustment to attain isothermal operation in the steady state.

THEORY

Mathematical model of a cluster thermocouple with three different bead sizes (see Fig. 1)

A. Assumptions

(a) The CO_2 and H_2O in the gas flow were less than 5% of the total gas. Gas heat radiation was therefore considered to be negligible.

(b) Heat conduction loss by the wires of the thermocouples was assumed to be negligible.

(c) Wall temperature T_w was assumed to be less than that of gas temperature T_g. Also, the diameters of the beads were assumed to vary as $d_1 < d_2 < d_3$, such that the thermocouple temperatures T_1, T_2, and T_3 could be ordered so that $T_g > T_1 > T_2 > T_3 > T_w$.

(d) Wall and thermocouple were assumed to have a blackbody of $\epsilon = 1$ and a shape factor of $F_{d\_w} = 1$.

(e) The system was assumed to be at equilibrium or $\partial T/\partial t = 0$.

(f) The flow was assumed to be laminar.

B. Heat balance for a thermocouple tree at equilibrium

$$\rho C_p \frac{dT}{dt} = q_{\text{convection}} - q_{\text{radiation}} = 0$$

and

$$q_{\text{convection}} = q_{\text{radiation}}$$

For the case of thermocouple bead 1

$$h_c(T_g - T_1) = \epsilon\sigma F_{d\_w}(T_1^4 - T_w^4)$$

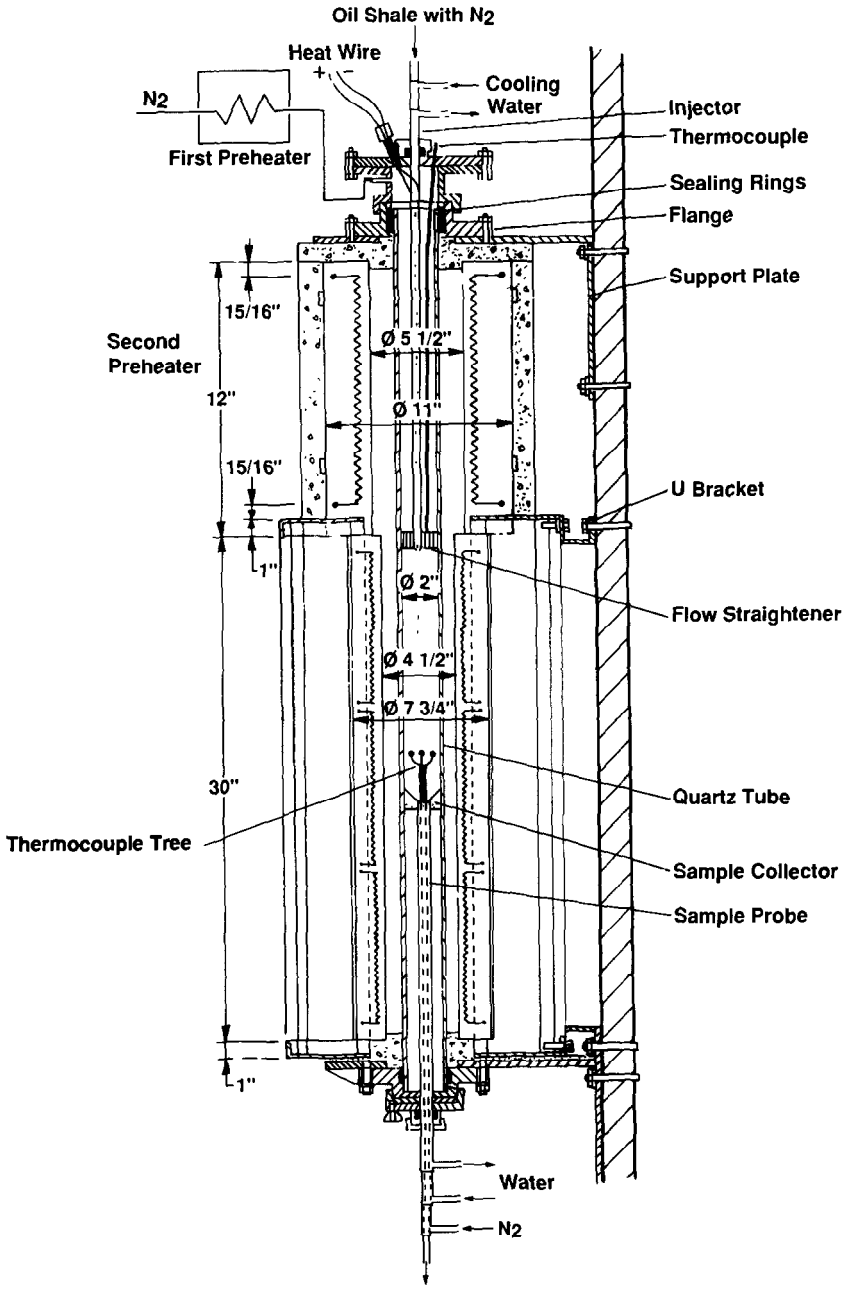

Fig. 1. Schematic diagram of the entrained reactor.

where the heat transfer of the laminar flow for spherical beads can be represented by

$$\mathrm{Nu} = \frac{h_c d_1}{k_f} = 2.0 + 0.6\ \mathrm{Re}^{0.5}\mathrm{Pr}^{0.33} = 2.0 + 0.6\left(\frac{U_g d_1}{\nu}\right)^{0.5}\mathrm{Pr}^{0.33}$$

and

$$h_c = \frac{\mathrm{Nu}\, k_f}{d_1} = 2\frac{k_f}{d_1} + 0.6\frac{\mathrm{Pr}^{0.33}k_f}{\nu^{0.5}}U_g^{0.5}d_1^{-0.5} = \frac{A}{d_1} + B\frac{\sqrt{U_g}}{\sqrt{d_1}}$$

Let $A = 2k_f$ and $B = 0.6\ \mathrm{Pr}^{0.33}k_f/\nu^{0.5}$.
Note: k_f, Pr and ν are functions of T_g, so the balance becomes

$$\left(\frac{A}{d_1} + B\frac{\sqrt{U_g}}{\sqrt{d_1}}\right)(T_g - T_1) = \epsilon\sigma\left(T_1^4 - T_w^4\right) \tag{1}$$

$$\left(\frac{A}{d_2} + B\frac{\sqrt{U_g}}{\sqrt{d_2}}\right)(T_g - T_2) = \epsilon\sigma\left(T_2^4 - T_w^4\right) \tag{2}$$

$$\left(\frac{A}{d_3} + B\frac{\sqrt{U_g}}{\sqrt{d_3}}\right)(T_g - T_3) = \epsilon\sigma\left(T_3^4 - T_w^4\right) \tag{3}$$

Here T_g, T_w and U_g are the unknowns that can be solved using eqns. (1), (2) and (3). By rearranging eqn. (1) as

$$T_w^4 = T_1^4 - \frac{1}{\epsilon\sigma}\left(\frac{A}{d_1} + B\frac{\sqrt{U_g}}{\sqrt{d_1}}\right)(T_g - T_1) \tag{4}$$

and substituting eqn. (4) into eqns. (2) and (3), we obtain

$$\left(\frac{A}{d_2} + B\frac{\sqrt{U_g}}{\sqrt{d_2}}\right)(T_g - T_2) = \epsilon\sigma\left(T_2^4 - T_1^4\right) + \left(\frac{A}{d_1} + B\frac{\sqrt{U_g}}{\sqrt{d_1}}\right)(T_g - T_1) \tag{5}$$

and

$$\left(\frac{A}{d_3} + B\frac{\sqrt{U_g}}{\sqrt{d_3}}\right)(T_g - T_3) = \epsilon\sigma\left(T_3^4 - T_1^4\right) + \left(\frac{A}{d_1} + B\frac{\sqrt{U_g}}{\sqrt{d_1}}\right)(T_g - T_1) \tag{6}$$

Subtracting eqn. (5) from eqn. (6), we obtain

$$A\left(\frac{T_g - T_3}{d_3} - \frac{T_g - T_2}{d_2}\right) + B\sqrt{U_g}\,\frac{T_g - T_3}{\sqrt{d_3}} - \frac{T_g - T_2}{\sqrt{d_2}} = \epsilon\sigma\left(T_3^4 - T_2^4\right)$$

$$B\sqrt{U_g} = \frac{\epsilon\sigma\left(T_3^4 - T_2^4\right) - A\left(\dfrac{T_g - T_3}{d_3} - \dfrac{T_g - T_2}{d_2}\right)}{\dfrac{T_g - T_3}{\sqrt{d_3}} - \dfrac{T_g - T_2}{\sqrt{d_2}}} \tag{7}$$

Rearranging eqn. (5) yields

$$A\left(\frac{1}{d_2}-\frac{1}{d_1}\right)+B\sqrt{U_g}\left(\frac{T_g-T_2}{\sqrt{d_2}}-\frac{T_g-T_1}{\sqrt{d_1}}\right)=\epsilon\sigma\left(T_2^4-T_1^4\right) \tag{8}$$

and substituting eqn. (7) into eqn. (8) provides the solution

$$A\left(\frac{1}{d_2}-\frac{1}{d_1}\right)+\frac{\epsilon\sigma\left(T_3^4-T_2^4\right)-A\left(\dfrac{T_g-T_3}{d_3}-\dfrac{T_g-T_2}{d_2}\right)}{\dfrac{T_g-T_3}{\sqrt{d_3}}-\dfrac{T_g-T_2}{\sqrt{d_2}}}\left(\frac{T_g-T_2}{\sqrt{d_2}}-\frac{T_g-T_1}{\sqrt{d_1}}\right)$$

$$=\epsilon\sigma\left(T_2^4-T_1^4\right) \tag{9}$$

C. List of symbols

d_1 diameter of small bead (cm)
T_1 temperature of small bead (K)
d_2 diameter of medium bead (cm)
T_2 temperature of medium bead (K)
d_3 diameter of large bead (cm)
T_3 temperature of large bead (K)
T_g gas flow temperature (K)
T_w wall temperature (K)
U_g gas flow velocity (cm s^{-1})
ϵ emissivity
F_{d-w} shape factor between beads and wall
h_c convection heat transfer coefficient (cal cm^{-1} K^{-1} s^{-1})
k_f gas conductivity (cal cm^{-1} K^{-1} s^{-1})
ν kinematic viscosity (cm^2 s^{-1})
Pr Prandtl number
Nu Nusselt number
Re Reynolds number
σ Stefan–Boltzmann constant, 5.729×10^{-12} (W cm^{-2} K^{-1} s^{-1})

EXPERIMENTAL

A schematic diagram of the reactor setup is shown in Fig. 1. Oil shale was entrained by a nitrogen carrier gas (primary gas) and introduced to the reaction zone using an injection probe. The injection probe outlet was located at the inlet of a Lindberg three-zone tube furnace maintained at reaction temperature. A preheated gas (secondary gas) contacted the entrained oil shale at the probe exit and heated the shale to the desired temperature. A quick-quench collection probe was used that traversed the

reaction zone. Both the injection probe and the collection probe were water-cooled, providing a well defined residence time within the reactor [5]. The position of the cooled collection probe was adjusted to control residence times [6]. The collection probe had temperature-measurement capabilities and was used to correlate gas temperatures inside the reactor tube to furnace temperatures around the heating element. One problem in measuring gas temperatures inside hot walls is that wall radiation interference can give faulty temperature readings. For this reason, a cluster thermocouple consisting of three thermocouples, each of a different bead size, was introduced through the collection probe. The diameters of the beads were 0.0438, 0.0812 and 0.133 cm. The three thermocouples were positioned at different locations inside the reactor tube to measure the temperature along the length of the reactor.

Flow visualization studies were performed in a 2 in inside diameter (ID) quartz tube cold model. The working fluid was air at room temperature, and the primary jet was made visible using tobacco smoke as a tracer to allow visual observation of the flow regimes within the reactor. A flow straightener with a ceramic honeycomb design was positioned in the secondary gas stream at the reactor inlet to provide a flat flow profile. These experiments were conducted by introducing smoke into the primary gas stream of the LFER model and observing the smoke pattern as the primary gas mixed with the secondary gas stream and flowed down the tubular reactor. Laminar, unsteady state and turbulent flow regions were identified using this technique. The geometry of the reactor system was made simple in design (1) to minimize the effect of mixing zones on residence time, and (2) to facilitate modeling of the flow.

RESULTS AND DISCUSSION

If kinetic rate data from reactor experiments are to be meaningful, identical treatment times are required for all particles. This in turn demands that dispersion of the central jet of oil shale be kept at a minimum. The present reactor was designed to provide both laminar flow and short residence times without any complications caused by mixing, dispersion, or particle wall interaction. Figure 2 shows photographs of typical flows produced in the reactor tube. In the steady laminar flow region, the central jet remained intact without significant spreading or dispersion throughout the furnace length. As the flow increased, the central jet began to break up, first in unsteady laminar fashion, and then becoming fully turbulent with rapid dispersion.

In order to extrapolate these cold flow studies to reaction temperatures, the results were presented in terms of the ratio of the average velocities of

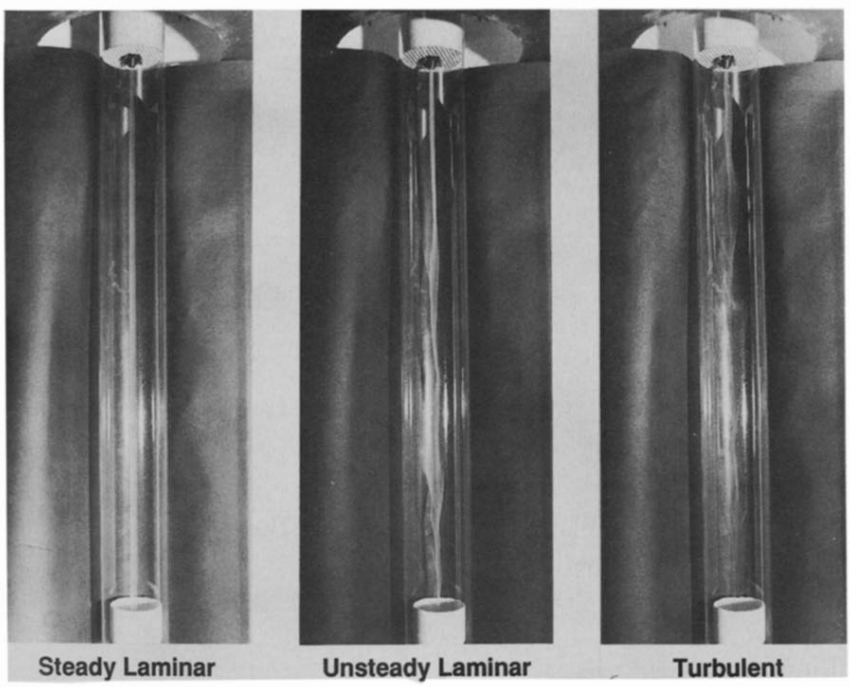

Fig. 2. Flow visualization in the entrained reactor.

the primary and secondary flows V_p/V_s vs. the Reynolds number of the secondary flow Re(S), where

$$V_p = \frac{Q_p}{\pi R_i^2}$$

$$V_s = \frac{Q_s}{\pi\left(R_t^2 - R_o^2\right)}$$

$$\mathrm{Re(S)} = \frac{2\rho_s V_s (R_t - R_o)}{\mu}$$

and Q_p and Q_s are the primary and secondary flow rates (l min^{-1}), respectively, R_i and R_o are the inside and outside radii (cm) of the injector, respectively, R_t is the inside radius (cm) of the reactor tube, ρ_s is the secondary inlet gas density (g cm^{-3}), and μ is the viscosity (g s^{-1} cm^{-1}).

Flow regimes, characterized visually at different flow ratios and Reynolds numbers, are plotted in Fig. 3. The curve, distinguishing the steady and unsteady laminar regions, gives the maximum Re(S) for which a steady laminar flow can be achieved as a function of V_p/V_s. Reactor inlet design and operating conditions have been found to have a dramatic influence on these flow regimes [4]. The observed flow profiles provided ample flexibility for altering the relative flow rates while maintaining good laminar flow. It

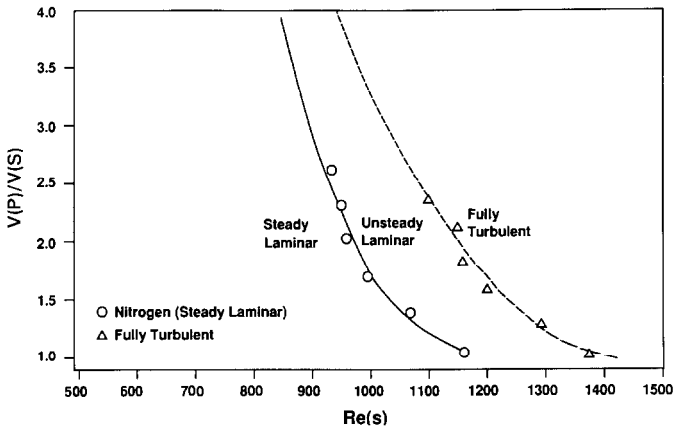

Fig. 3. Flow regimes in laminar flow entrained reactor.

was found that the inlet must be followed by a flow straightener with sufficient pressure loss to produce a nearly uniform flow. These conditions were met by Kobayashi [6], who confirmed that coal particles remain near the axis. These results apply directly to a heated reactor as long as isothermal conditions prevail.

The temperature of the system was characterized using the three thermocouples of different bead sizes. Since radiative heat transfer between the thermocouple beads and the reactor wall increases with increasing bead size, the three thermocouples can indicate different temperatures under the same environment. When the gas temperature was higher than the wall temperature, the thermocouple with a larger bead had a lower temperature than that with a smaller bead. This was because its radiative heat transfer to the wall was larger than the convective heat transfer from the hot gas. However, when the gas temperature was lower than the wall temperature, the thermocouple with a larger bead had a higher temperature than that with a smaller bead.

A mathematical model was used to calculate the wall and gas temperatures based on the temperature measurements of the three thermocouples. Figure 4 shows the wall and gas temperatures along the length of the reactor tube with the furnace temperature at 600 °C without a water-cooled probe. The flow rates of the primary (P) and secondary (S) gases were 0.4 and 13 l min^{-1}, respectively. The preheated entraining gas temperature was 815 °C. The results indicated that the difference between the gas and wall temperatures was minimal. Therefore, all temperatures within each given reactor zone were essentially isothermal. Furthermore, the remaining length of the reactor tube was isothermal with the exception of a 2 in zone at each end. If the flow rates of the primary and secondary gases were raised to 1.0 and 20 l min^{-1}, respectively, leading to a lower temperature of the preheated entraining gas, the wall temperatures became higher than the gas temperatures all

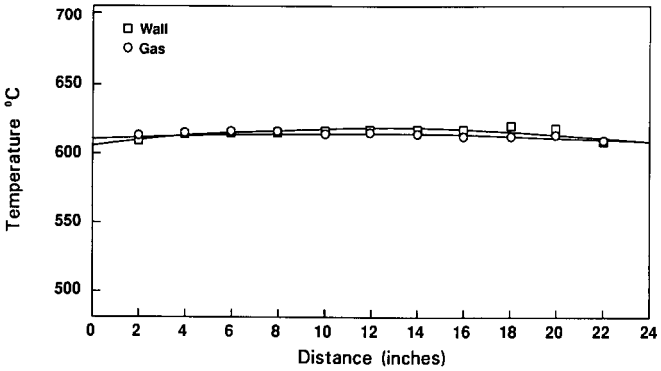

Fig. 4. Temperatures of gas and wall in LFER vs. distance. Flow rates, 0.4 (P), 13 (S) l min^{-1}; furnace temperature, 600 °C; preheater temperatures, 565 °C (no. 1), 815 °C (no. 2).

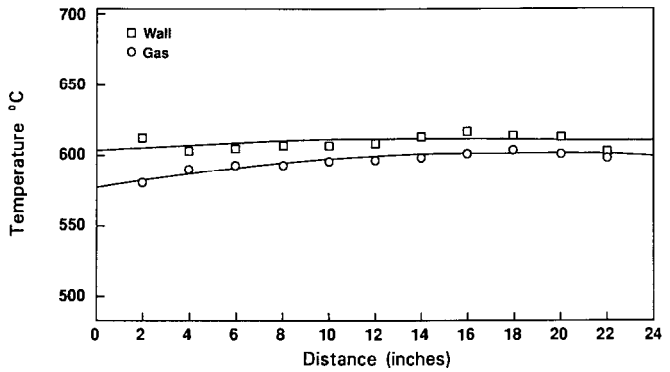

Fig. 5. Temperatures of gas and wall in LFER vs. distance. Flow rates, 1 (P), 20 (S) l min^{-1}; furnace temperature, 600 °C; preheater temperatures; 565 °C (no. 1), 815 °C (no. 2).

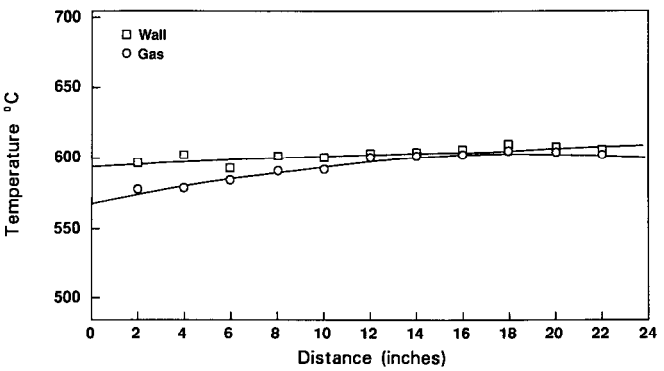

Fig. 6. Temperatures of gas and wall in LFER vs. distance. Flow rates, 1 (P), 20 (S) l min^{-1}; furnace temperature, 600 °C; preheater temperatures; 565 °C (no. 1), 870 °C (no. 2).

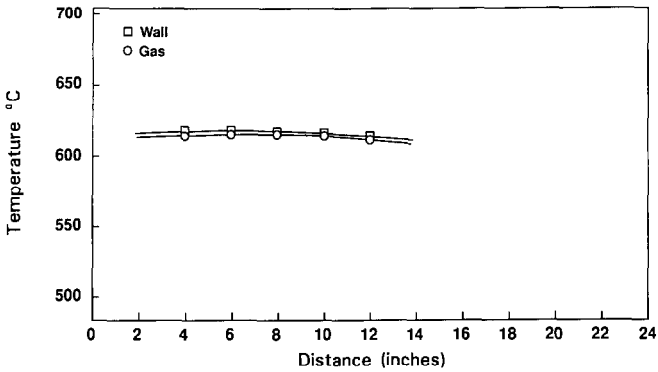

Fig. 7. Temperatures of gas and wall in LFER vs. distance. Flow rates, 0.4 (P), 13 (S) l min^{-1}; furnace temperature, 600 °C; preheater temperatures; 565 °C (no. 1), 815 °C (no. 2).

along the reactor (Fig. 5). However, the temperatures of the furnace and the entraining gas can be independently controlled to provide isothermal operation. When the temperature of the preheated entraining gas was raised to 870 °C (Fig. 6), the gas and wall temperatures were similar to those shown in Fig. 5. It should be possible to adjust the entraining gas temperature or the furnace temperature to maintain an isothermal condition.

Similar results were observed with the water-cooled probes in their appropriate positions. Figure 7 shows the wall and gas temperatures of the two upper zones with the water-cooled probe located in the center of the bottom zone of the three-zone furnace. Again, the temperatures within a given zone were essentially isothermal, and the zones along the reactor length were also isothermal.

SUMMARY

Flow visualization and temperature characterization in an entrained flow reactor have provided the data necessary to proceed with a kinetic study on the rapid pyrolysis of oil shale. Calibration curves depicting the flow regimes have confirmed that the existing inlet and reactor design can be operated without particle dispersion caused by turbulence. A thermocouple tree has also been successfully utilized to identify the conditions necessary for isothermal furnace operation. This technique has been modeled, and a comparison of the wall temperature to the gas temperature shows that the wall or gas heaters can be easily adjusted to obtain the desired heating conditions.

REFERENCES

1 H.W. Johns, E.E. Jukkola and W.I.R. Murphy, Development and Operation of an Experimental Entrained-solids, Oil–Shale Retort, Bureau of Mines Report of Investigations 5522, 1959.
2 M. Steinberg and P.T. Fallon, Flash Pyrolysis of Oil Shale with Various Gases, The Oil Shale Symposium, 188th National American Chemical Society Meeting, St. Louis, Missouri, April, 1984.
3 D.R. Kahn, A.Y. Falk and M.P. Garey, Flash Hydropyrolysis of Eastern Oil Shale, Proc. 1983 Eastern Oil Shale Symposium, November 13–16, Lexington, Kentucky, 1983, University of Kentucky Institute for Mining and Minerals Research, Lexington, Kentucky.
4 R.J. Flaxman and William L.H. Hallett, Fuel, 66 (1987) 607.
5 S. Badzioch and P.G.W. Hawksley, Ind. Eng. Chem. Des. Dev., 9 (1970) 521.
6 H. Kobayashi, Devolatilization of Pulverized Coal at High Temperatures, Ph.D. thesis, Massachusetts Institute of Technology, Cambridge, Massachusetts, 1976.